# The Effects of Linking Substituents on the *In Vivo* Behavior of Site-directed, Peptide-based, Diagnostic Radiopharmaceuticals

ADAM F. PRASANPHANICH[1,3], STEPHANIE R. LANE[8], SAID D. FIGUEROA[1], LIXIN MA[1,3,4,5,6], TAMMY L. ROLD[3,4,5], GARY L. SIECKMAN[3], TIMOTHY J. HOFFMAN[3,4,5], JOSEPH M. MCCRATE[1] and CHARLES J. SMITH[1,2,3,5,7*]

*[1]Department of Radiology, [2]University of Missouri Research Reactor Center, [4]Department of Internal Medicine, [5]The Radiopharmaceutical Sciences Institute, [6]International Institute of Nano and Molecular Medicine and [7]Department of Medical Pharmacology and Physiology, University of Missouri-Columbia School of Medicine, Columbia, Missouri, 65211; [3]Research Division, Harry S. Truman Memorial Veterans' Hospital, Columbia, Missouri, 65201; [8]Department of Chemistry, University of Missouri-Columbia, Columbia, Missouri, 65211, U.S.A.*

**Abstract.** *A number of human cancers are known to over-express the gastrin-releasing peptide receptor (GRPr) on cell surfaces. The high specificity and affinity of bombesin (BBN), an amphibian analogue of mammalian gastrin-releasing peptide, for the GRPr makes it an ideal candidate for delivery of diagnostic probes, such as $^{99m}$Tc radiometal, to tumor sites. An optimized targeting agent possesses high tumor uptake with minimal uptake in normal tissues. In this study, $^{99m}$Tc-targeting vectors of bombesin using various amino acid/aliphatic pharmacokinetic modifiers or linking groups were evaluated to determine the effect of the spacer on receptor binding affinity, internalization/externalization and biodistribution. Conjugates of the general type [DPR-X-BBN] (X = amino acid/aliphatic pharmacokinetic modifier) were synthesized by solid phase peptide synthesis (SPPS) and metallated with either low-valent, radioactive Tc-99m(I) or non-radioactive Re(I)-tricarbonyl precursors. All of the new non-metallated and metallated conjugates were characterized by electrospray ionization mass spectrometry (ESI-MS). Receptor binding affinity, internalization/externalization and biodistribution studies in normal (CF-1) and tumor (human prostate PC-3-bearing mice) are reported. The effectiveness of targeting xenografted PC-3 tumors in rodents for two of the new $^{99m}$Tc-BBN conjugates is demonstrated herein using small animal single photon emission computed tomography (SPECT).*

*Correspondence to:* Dr. Charles J. Smith, Harry S. Truman Memorial VA Hospital, Research Service Room A005, 800 Hospital Drive, Columbia, MO 65201, U.S.A. Tel: +573 814 6000 ext. 3683, Fax: +573 882 1663, e-mail: smithcj@health.missouri.edu

*Key Words:* Bombesin, gastrin-releasing peptide, 2,3-diaminopropionic acid, spacer, tethering moiety, PC-3, Tc-99m, site-directed, receptor, diagnostic radiopharmaceuticals, SPECT, MRI, CT, pharmacokinetics.

Radiolabeled, site-directed targeting vectors or biologically-active conjugates (*i.e.*, peptides, small proteins, antibody fragments, or intact antibodies) continue to hold some promise for early diagnosis or treatment of human disease (1-15). For example, specifically targeting cell-surface receptors that tend to be over-expressed on human cancer cells offers the advantage of identifying and treating specific diseased human tissue with minimal collateral damage to neighboring, normal tissues (1-15). Radiolabeled targeting vectors (Figure 1) for treatment of human disease are comprised of 1) a targeting vector, 2) a pharmacokinetic modifier (often a aliphatic or amino acid linker/tethering moiety), 3) a bifunctional chelating agent (a chelating ligand that is able to stabilize the radioactive metal center under *in vivo* conditions while covalently linking the radiometal/ligand complex to the targeting vector) and 4) a radiometal (a diagnostic ($\gamma$ or $\beta^+$) or therapeutic ($\beta^-$ or $\alpha$) radionuclide) (5, 6). There is much impetus into the design of new and improved targeting vectors and better treatment strategies based upon site-directed drugs of this general type. For example, identifying specific structural features that influence the ability of the conjugate to effectively clear the bloodstream, target specific tissue and be rapidly cleared *via* the renal/urinary or hepatobiliary excretion routes is very important.

Radiolabeled antibodies have demonstrated the potential to be used as site-directed, biologically active compounds for development of new and successful diagnostic and therapeutic radiopharmaceuticals for human cancers (5, 11-15). However,

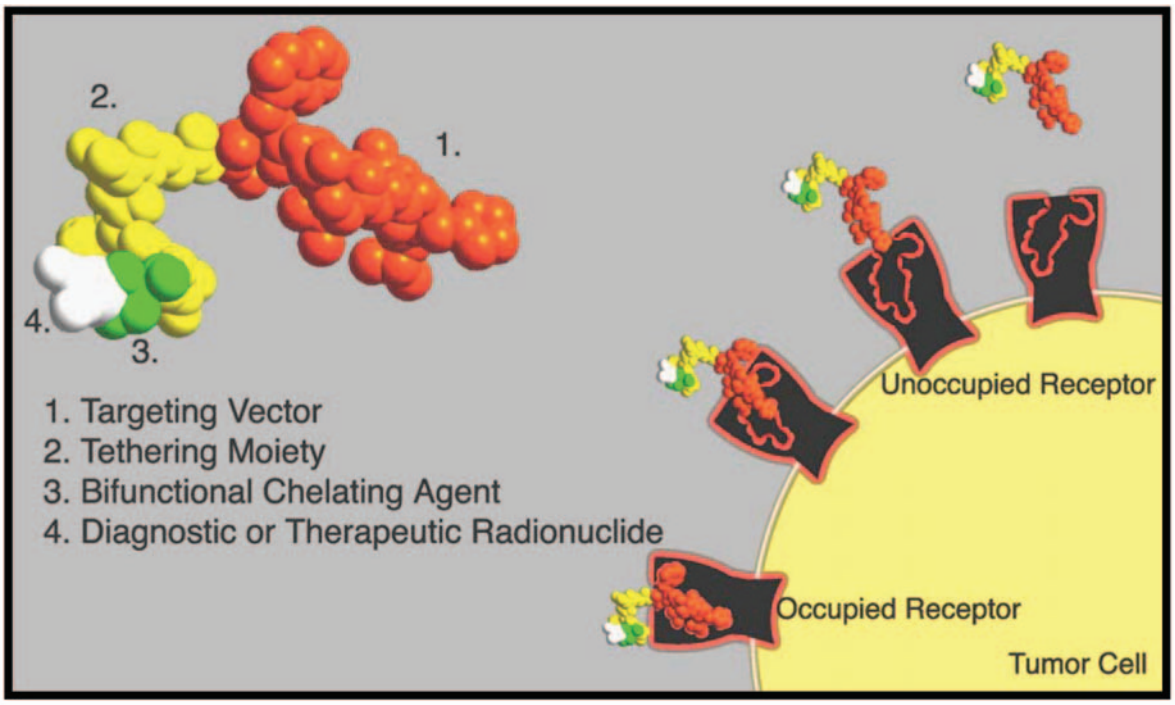


Figure 1. *Overview of components constituting a site-directed radiopharmaceutical. (1) Targeting Vector, orange. (2) Tethering Moiety, yellow. (3) Bifunctional Chelating Agent, green. (4) Diagnostic or Therapeutic Radionuclide, white.*

antibodies suffer from very slow clearance from blood serum/non-target tissue and the less-than-desirable tumor uptake, limiting the clinical effectiveness of these targeting vectors (5, 11-15). Lower molecular weight, receptor-specific peptides, on the other hand, can be more suitable for delivery of diagnostic or therapeutic radionuclides to antigen binding sites when compared to antibodies. Peptides offer distinct advantages such as rapid clearance from whole blood, ease of penetration into the tumor vascular endothelium and more rapid excretion from the human body (5, 8). As a result of their small size, receptor-avid peptides possess relatively low immunogenicity (5, 8). Lastly, high affinity receptors, selectively over-expressed on a variety of neoplastic cells have been identified for a number of small, receptor-avid peptides making them ideal candidates as new diagnostic and/or therapeutic radiopharmaceuticals (1-10).

The use of spacer group technology can be a critical element of design for development of site-directed radiopharmaceuticals. Linker groups such as aliphatic hydrocarbon or amino acid spacers are strategically placed at a point between the bifunctional chelating ligand and the antigen-specific region of the targeting vector so that biological integrity or receptor specificity of the molecule is preserved (16-21). Specific linkers can also be used as pharmacokinetic modifiers to chemically tune the hydrophilicity/hydrophobicity of the radiometallated conjugates and, hence, excretion either the renal/urinary or hepatobiliary excretion pathway (5, 20, 21). Use of "innocent" peptide sequences, such as polylysine, glycine, or aspartic acid residues into the peptide sequence serves well to increase the hydrophilic nature of the conjugate promoting excretion primarily the renal/urinary system (5, 21). On the other hand, more hydrophobic pharmacokinetic modifiers produce hydrophobic conjugates that accumulate in liver tissue and are excreted primarily *via* the hepatobiliary pathway (20, 21).

Central to the design of site-directed radiopharmaceuticals is also development or choice of specific ligand frameworks that stabilize the metal center under *in vivo* conditions. Poly(aminocarboxylic acids) tend to provide kinetically inert, *in vivo* stable conjugates radiolabeled with copper, lanthanide, or lanthanide-like elements (22-24). On the other hand, heteroatomic donor ligands have been shown to stabilize technetium, rhenium and other radionuclides in numerous oxidation states (25-33).

Lastly, the choice of radioelement is equally important for diagnostic imaging or delivery of a cytotoxic radiation dose to the tumor tissue for therapy. Ideally, radionuclides should be readily available and possess a physical half-life very similar to the biological half-life of the targeting vector. Emission of a single gamma (γ) photon in the 100-250 keV range is ideal for SPECT (single photon emission computed tomography)

imaging (34). For example, Tc-99m, the single most used radionuclide in diagnostic imaging, emits a single 140 keV gamma photon. PET (positron emission tomography) imaging radiometals, on the other hand, utilize positron-emitting ($\beta^+$) radionuclides for diagnostic purposes. Positron emitting radionuclides produce two 511 keV gamma photons emitted at angles of 180˚ that can be identified by coincidence counting over many angles around the body (24). Radionuclides for therapy are generally either $\beta^-$ or $\alpha$-emitting radionuclides. Examples of radionuclides for targeted therapy include Lu-177, Sm-153, Cu-64, Pm-149, Y-90 and At-211 (6, 35, 36).

In recent years, our group and others have been interested in the development of radiolabeled targeting vectors having very high selectivity and affinity for GRP receptors that are over-expressed on human cancer tissues such as prostate, breast, pancreatic and small cell lung cancers (7, 9). Our investigations have led us to develop specific targeting vectors that are potentially useful for diagnosis or treatment of disease (10, 16-19, 21). More recently, we have described the synthesis of GRP receptor-specific conjugates containing bi- and tridentate, aliphatic and aryl amines for co-ordination to the *fac* $[^*M(CO)_3]^+$ metal center ($^*M$ = $^{186/188}Re$ or $^{99m}Tc$) (10, 16, 21). In these studies, we have shown that bidentate diaminopropionic acid or tridentate pyrazolyl-primary amine chelating ligand frameworks provide for *in vitro* and *in vivo* kinetically inert $^{99m}Tc$-GRP conjugates with very high selectivity and affinity for receptors over-expressed on human, prostate PC-3 cancer cells (10, 16, 21). The *fac*-$[^{99m}Tc(CO)_3(H_2O)_3]^+$ precursor has received considerable interest as of late for radiolabeling of biomolecular targeting vectors due in part to its availability *via* kit preparation (IsoLink®), the substitution lability of appending aquo ligands for numerous co-ordinating donor atoms and the relative kinetic and thermodynamic stability of prepared complexes (10, 16, 21, 30, 31). Herein we report a new series of GRP conjugates containing the N-terminal diaminopropionic acid chelator (10, 16) that is easily radiolabeled with *fac*-$[^{99m}Tc(CO)_3(H_2O)_3]^+$ *via* the IsoLink® radiolabeling kit. These new conjugates demonstrate very high affinity for the GRP receptor in normal and tumor-bearing mice. This comprehensive report describes in detail the influence of pharmacokinetic modifier on specific GRP receptor uptake of radiolabeled ligand. *In vivo* SPECT molecular imaging studies in rodents bearing human, PC-3, xenografted tumors are presented.

## Materials and Methods

An Applied Biosystems 432A peptide synthesizer was used for SPPS of the BBN derivatives employing traditional Fmoc procedures. Post-synthesis procedures include cleavage, purification and ESI-MS for isolation and identification of peptide conjugates in high purity. Reverse-phase high performance liquid chromatographic (RP-HPLC) analyses were performed on a Waters 600E system equipped with a Waters 2487 dual wavelength absorbance detector, an in-line EG&G ORTEC NaI crystal scintillation detector, an Eppendorf CH-30 column heater and a Hewlett Packard 3395 integrator. RP-HPLC solvents were purchased as RP-HPLC grade from Fisher Scientific (Pittsburg, PA). ESI-MS analyses were performed by SynBioSci (Livermore, CA). $^{99m}Tc$, in the chemical form $Na^{99m}TcO_4$, was eluted from a $^{99}Mo/^{99m}Tc$ generator provided by Bristol-Myers Squibb. $[^{99m}Tc(H_2O)_3(CO)_3]^+$ was prepared by addition of sodium pertechnetate to IsoLink® radiolabeling kits provided by Tyco Healthcare (St. Louis, MO). $[Re(Br)_3(CO)_3]^{2-}$ was prepared according to the literature and used without further purification (37). All other chemicals were purchased at the appropriate grade from Aldrich Chemical Company (St. Louis, MO, USA).

*In vivo* and *in vitro* studies were used to determine the efficacy of the $[^{99m}Tc(H_2O)(CO)_3$-DPR-X-BBN$]^+$ derivatives as potential radiopharmaceuticals and to compare and contrast *in vivo*/*in vitro* activity. *In vitro* cell binding affinity, internalization and efflux studies were conducted to determine the cellular uptake and activity of the new BBN derivatives. *In vivo* studies in normal (CF-1) (Charles River, Wilmington, MA, USA) or severely compromised immunodeficient (SCID) mice (Taconic, Germantown, NY, USA) were used to determine the pharmacokinetic properties and biodistribution of radioactivity for all of the new $^{99m}Tc$-conjugates. All animal studies were conducted in accordance with the NIH guide for Care and Use of Laboratory Animals, as well as the Policy and Procedures for Animal Research at the Harry S. Truman Memorial Veterans' Hospital. Animals were anesthetized prior to injections with isoflurane (Baxter Healthcare Corporation, Deerfield, IL, USA) at a rate of 2.5% with 0.4 L of oxygen through a non-rebreathing anesthesia vaporizer. Mice were euthanized by inhalation of carbon dioxide in a closed chamber. *In vivo* molecular imaging procedures took place on a Varian Unity Inova MRI system and Siemens Medical Systems microCAT II capable of micro-SPECT /micro-CT imaging.

*Solid-phase peptide synthesis of DPR-X-BBN derivatives.* Solid-phase peptide synthesis of DPR-X-BBN conjugates took place on an Applied Biosystems Model 432A automated peptide synthesizer utilizing traditional Fmoc protection chemistry. Fmoc-protected amino acids and amino acid derivatives possessing appropriate side-chain protections and rink amide MBHA resin were used in quantities according to synthesizer specifications to synthesize DPR-X-BBN conjugates of the form DPR-X-Gln-Trp-Ala-Val-Gly-His-Leu-Met-($NH_2$) where X=NNN, NNN-βAla, NNN-5Ava, RRR, RRR-βAla, RRR-5Ava and SSS (N, R and S = asparagine, arginine and serine, respectively). Products were cleaved and deprotected according to standard procedure using a 2:1:1:36 thioanisol, water, ethanedithiol and trifluoroacetic acid cocktail. The resin was removed from the solution and the solution was precipitated in methyl-t-butyl ether. The crude peptide was purified by RP-HPLC. Solvents were removed *in vacuo* using a Labconco CentriVap vacuum centrifugation system. Quality control RP-HPLC was used to determine the final purity of the collected products. ESI-MS was used to determine the molecular weight of the purified peptide derivatives.

*Reverse-phase high performance liquid chromatography.* Reverse-phase high performance liquid chromatography was performed using acetonitrile as the organic phase and water as the aqueous

phase. A Phenomenex analytical reversed phase C18 column (50x4.6 mm, 5 μm) was used for chromatographic retention and separation of injected samples. The aqueous (Water, Solvent A) and organic (Acetonitrile, Solvent B) solvents were used in solution containing 0.1% trifluoroacetic acid. A linear gradient consisting of 95% A:5% B at time zero and 20% A:80% B at 20 m followed by isocratic flow at 20% A:80% B for 5 m was used. The system was then returned to its initial conditions and allowed to run for 5 m to allow for the system to re-equilibrate. A constant flow rate of 1.5 mL per minute was maintained throughout the sample run and re-equilibration period. The chart speed of the integrator was 0.5 cm per minute. Column temperature was maintained at 34˚C. Absorbance detection was observed at a wavelength of 280 nm. The presence of an inline NaI solid scintillation detector allowed for analyses of the new radiolabeled conjugates.

*Synthesis of Re-DPR-X-BBN derivatives.* To 10 mg of DPR-X-BBN peptide in water was added excess $[Re(Br)_3(CO)_3]^{2-}$. The reaction mixture was heated for 1 h at 80˚C. Identification of product and product purification were carried out *via* RP-HPLC. Solvent was removed by vacuum centrifugation and quality control of purified conjugates was performed by RP-HPLC analysis. ESI-MS was used to determine the molecular weight of the $[Re(CO)_3(H_2O)$-DPR-X-BBN$]^+$ conjugates.

*$^{99m}$Tc radiolabeling of DPR-X-BBN derivatives.* $[^{99m}Tc(H_2O)(CO)_3$-DPR-X-BBN$]^+$ conjugates were prepared in aqueous solution. Briefly, $[fac\text{-}^{99m}Tc(CO)_3(H_2O)_3]^+$ was prepared in an IsoLink® radiolabeling kit by addition of 1 mL of generator eluent to the reaction vial and heating for 20 m. The kit vial was opened and 0.120 mL of 0.1 M HCl added. [DPR-X-BBN] (100 μg (~5 nmol)) was reacted with 0.5 mL of the IsoLink® radiolabeling kit solution ($[fac\text{-}^{99m}Tc(CO)_3(H_2O)_3]^+$) for 1 h at 80˚C. Purification of conjugate from the reaction mixture was performed using RP-HPLC, collecting into aliquots containing 100 μL of 1 mg/mL bovine serum albumin (BSA). Products were assayed for quality control purposes (RP-HPLC) immediately following collection and removal of acetonitrile RP-HPLC solvent from solution. *In vitro* and *in vivo* studies were performed using high specific activity radiolabeled conjugates that were collected and purified *via* RP-HPLC.

*Time point and in vitro human serum stability studies of $[^{99m}Tc(H_2O)(CO)_3$-DPR-X-BBN$]^+$ conjugates.* Time point stability studies were performed using high specific activity conjugate collected off of the RP-HPLC. Acetonitrile was removed from the collected solution *via* nitrogen stream and the eluent was then allowed to sit for 1, 3 and 5 h periods at ambient temperature in aqueous solutions containing BSA. Analytical RP-HPLC was then used to observe the stability of the radiometal BBN-ligand framework.

The stability of the $^{99m}$Tc-radiolabeled [DPR-X-BBN] conjugates was determined in human serum at 1, 3 and 5 h time point incubation periods. The RP-HPLC radiolabeled conjugate (3 equivalents by volume) was added to human serum (1 equivalent by volume) and allowed to incubate for 1, 3 and 5 h intervals at 37˚C in a $CO_2$ saturated atmosphere. At the specific time point, the serum-conjugate mixture was analyzed by thin layer chromatography (TLC) as well as RP-HPLC. The TLC was conducted using water and acetone mobile phases and silica gel as the stationary phase. In both systems, the plate was spotted with the reaction mixture and allowed to develop in saturated chambers. The plate was cut in half and counted in a scintillation well counter. An analytical sample injection of the mixture was run *via* RP-HPLC to observe stability of the radiolabel in solution containing human serum.

*In vitro receptor affinity studies.* The inhibitory concentration 50% ($IC_{50}$) values of the $[Re(H_2O)(CO)_3$-DPR-X-BBN$]^+$ derivatives, where X=NNN, NNN-βAla, NNN-5Ava, RRR, RRR-βAla and RRR-5Ava, were determined by a competitive displacement binding assay using $^{125}$I-Tyr$^4$-BBN as the radiolabeled displacement ligand. Briefly, $3x10^6$ PC-3 cells were incubated with 20,000 cpm $^{125}$I-Tyr$^4$-BBN and increasing concentrations of $[Re(H_2O)(CO)_3$-DPR-X-BBN$]^+$ solutions for 37˚C for 1 h. The cell media, D-MEM/F-12K, consisted of 0.01 M MEM and 2% BSA at pH 5.5. Following incubation, the reaction medium was aspirated and the cells washed four times with media. The final cell media was aspirated and radioactivity counted. All *in vitro* cell-associated radioactivities were determined by counting of the washed cells in a Packard Riastar multi-well gamma counting system.

*In vitro internalization and efflux studies.* The internalization and efflux analysis of $[^{99m}Tc(H_2O)(CO)_3$-DPR-X-BBN$]^+$ conjugates, where X=NNN, NNN-βAla, NNN-5Ava, RRR, RRR-βAla and RRR-5Ava, were performed by incubation of conjugates in PC-3 cells and counting of internalized radioactivity at various time points. Internalization analyses were performed by incubation of approximately $3x10^6$ PC-3 cells with 20,000 cpm of $[^{99m}Tc(H_2O)(CO)_3$-DPR-X-BBN$]^+$ for 1 h at 37˚C for 15, 30, 45, 60, 90 and 120 m time points. The cell media was aspirated and cells washed four times after incubation. The cells were washed with 0.2 N acetic acid/0.5 M NaCl at pH 2.5 to remove surface-bound radioactivity. The percentage of internalized radioactivity was counted and plotted *versus* incubation time. Efflux analysis was performed on cells after an initial 45 m internalization period after which the cells were washed three times with buffer solution at room temperature and again suspended into solution for further incubation. Secondary incubation periods of 0, 15, 30, 45, 60 and 90 m post-internalization was followed by an initial wash in cold buffer of the cells, followed by a washing with acetic acid/saline solution at pH 2.5 at 4˚C to determine the extent of radioactive efflux. Internalized radioactivity was then counted as percentage of cell-associated radioactivity and plotted *versus* incubation time.

*Biodistribution studies in CF-1 normal mouse models.* Normal mouse models of the CF-1 type were used to determine the *in vivo* biodistribution of $[^{99m}Tc(H_2O)(CO)_3$-DPR-X-BBN$]^+$ conjugates, where X=NNN, NNN-βAla, NNN-5Ava, RRR, RRR-βAla and RRR-5Ava. The mice were injected *via* the tail vein with 5 μCi of conjugate in 100 μL isotonic saline. At 1 h post-intravenous (*p.i.*) injection, the mice were euthanized. Subsequently, the tissues and organs were excised, weighed and radioactivity counted in a NaI crystal scintillation well counter. The percent dose internalized (%ID) and percent dose internalized per gram (%ID/g) were calculated. The value for urine was determined as %ID from collected urine, urine deposited on cage paper, and activity in the bladder. Blood values were estimated assuming a whole-blood volume of 6.5% whole body weight. Additional studies with 4 and 24 h *p.i.* time periods were conducted using $[^{99m}Tc(H_2O)(CO)_3$-DPR-NNN-5Ava-BBN$]^+$ and $[^{99m}Tc(H_2O)(CO)_3$-DPR-NNN-βAla-BBN$]^+$.

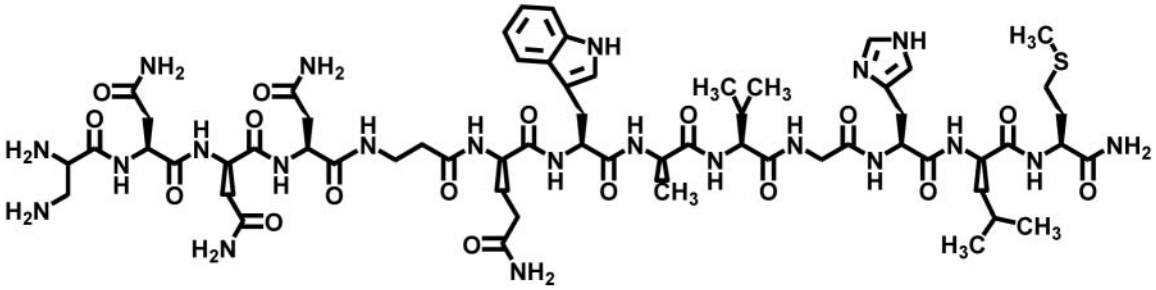

Figure 2. *Structure of DPR-NNN-βAla-Gln-Trp-Ala-Val-Gly-His-Leu-Met-NH$_2$.*

*Biodistribution studies in PC-3 tumor-bearing SCID mouse models.* Tumor-bearing SCID mice bearing xenografted human, PC-3, prostate tumors were used to determine *in vivo* tumor accumulation, biodistribution and pharmacokinetics of $[^{99m}Tc(H_2O)(CO)_3$-DPR-NNN-βAla-BBN$]^+$ conjugate. Female SCID outbred mice were purchased from Taconic (Germantown, NY). The mice were housed five animals per cage in sterile microisolator cages in a temperature and humidity controlled room with a 12 h light/12 h dark schedule. The mice were fed water *ad libitum* and autoclaved rodent feed (Ralston Purina Company, St. Louis, MO, USA). Human prostate PC-3 cells were injected in the bilateral subcutaneous flank in a suspension of 100 μL sterile saline per injection site. The cells were allowed to grow *in vivo* for 2-3 weeks post-inoculation. At the time of the studies, tumor size ranged from 0.09 to 0.41 grams. Intravenous injection of 5 μCi of the radiolabel in 100 μL isotonic saline was followed by euthanasia of the mice at 1, 4 and 24 h *p.i.* time intervals. Determination of %ID and %ID/g in tissues was performed as previously described (*vide supra*).

*SPECT/CT & MRI imaging.* Tumor-bearing SCID mice bearing xenografted human, PC-3, prostate tumors were intravenously injected with ~2 mCi $[^{99m}Tc(H_2O)(CO)_3$-DPR-NNN-βAla-BBN$]^+$ or $[^{99m}Tc(H_2O)(CO)_3$-DPR-SSS-BBN$]^+$. At 24 h *p.i.*, the mice were euthanized. The mice were immediately placed prone in a house-built cradle for performing imaging studies using magnetic resonance imaging (MRI) and SPECT/CT. MRI images of tumor bearing animals were acquired in order to correlate the relative uptake degree to the mouse anatomical features. Diffusion weighted spin echo multi-slice images were acquired on 7T/210mm Varian Unity Inova MRI system equipped with a quadrature driven birdcage coil (38 mm ID) (Varian Inc., Palo Alto, CA, USA). The following parameters were used: repetition time (TR)/echo time (TE) = 2000 msec/37 msec, b factor = 734 s/mm$^2$, diffusion gradients in x, y and z directions, 7-11 slices, slice thickness of 1 mm with no gap, image matrix size = 256x256, field of view (FOV) = 30 mm x 30 mm, number of averages = 2. A fast spin echo multislice sequence was used to collected coronal images with parameters of TR/TE = 2000 msec/13 msec, slice thickness = 1 mm with no gap, image matrix = 512x256, FOV = 70 mm x 30 mm, number of average = 2. The Micro- SPECT/CT is a combined modality unit equipped with dual pixilated SPECT detectors each coupled to a square 3x3 array of position sensitive photomultiplier tubes. The CT component consists of a CCD X-ray detector and an 80 kVp micro-focus X-ray source (40 μm focal spot). At 24 h *p.i.*, micro-SPECT imaging was performed using a symmetrical 20% $^{99m}$Tc photopeak discriminating window. Micro-SPECT data was collected over rotations totaling 360˚, 60 step acquisition with a 2 mm pinhole collimator. Micro-CT data acquisition was collected prior to SPECT data acquisition for the purpose of anatomic/molecular data fusion. Micro-CT imaging was performed for 8 m and concurrent image reconstruction was achieved with the use of a Fanbeam (Feldkamp) Filtered back projection algorithm. Pinhole tomographic reconstructed $^{99m}$Tc SPECT data was generated using a 3D-OSEM algorithm with software corrections applied for pinhole misalignments. A Gaussian 1.2 FWHM filter was applied to the reconstructed SPECT data. The SPECT data was visualized and fused with the corresponding CT data with the advanced 3D visualization AMIRA 3.1 software (Mercury, USA).

## Results

Synthesis of the [DPR-X-BBN] conjugates, where X=NNN, NNN-βAla, NNN- 5Ava, RRR, RRR-βAla, RRR-5Ava and SSS, (Figure 2) by SPPS followed by purification by RP-HPLC provided conjugates of very high purity as determined by analytical RP-HPLC and electrospray ionization mass spectrometry. Approximately 80% yield was obtained. Experimental data from ESI-MS analyses of the [DPR-X-BBN] conjugates (1368.8, 1439.6, 1467.9, 1495.7, 1566.3, 1594.5 and 1287.8) correspond to calculated values (1368.5, 1439.6, 1467.7, 1495.8, 1566.9, 1594.9 and 1287.4) as determined for X=NNN, NNN-βAla, NNN-5Ava, RRR, RRR-βAla, RRR-5Ava and SSS, respectively. The high purity conjugates, existing as clean white solids, were used in subsequent labeling reactions with Re and $^{99m}$Tc metal precursors.

Rhenium-metallated BBN conjugates were prepared by addition of excess $[Re(Br)_3(CO)_3]^{2-}$ to [DPR-X-BBN] conjugates, where X=NNN, NNN-βAla, NNN-5Ava, RRR, RRR-βAla and RRR-5Ava, in aqueous solution. Subsequent purification *via* RP-HPLC and dried under evacuated centrifugation afforded the pure conjugates as white solids. Experimental ESI-MS data (1638.9, 1710.4, 1737.3, 1764.9, 1863.4 and 1835.4) very closely matches the calculated values (1638.8, 1710.4, 1737.7, 1763.3, 1863.1 and 1835.1) for all of the Re-conjugates. RP-HPLC retention

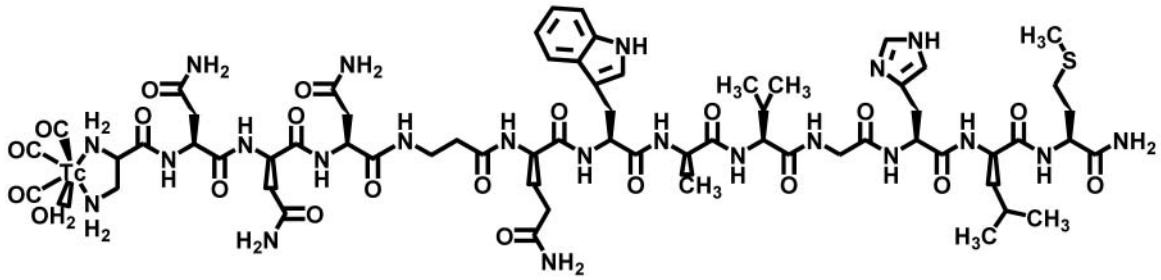

Figure 3. *Structure of* $[^{99m}Tc(CO)_3(H_2O)$-DPR-NNN-βAla-Gln-Trp-Ala-Val-Gly-His-Leu-Met-$NH_2]^+$.

times of $t_R$=14.0, 13.4, 13.5, 12.3, 12.3 and 12.4 m correspond to Re-conjugates where X=NNN, NNN-βAla, NNN-5Ava, RRR, RRR-βAla and RRR-5Ava, respectively. Stability of the M(I)-N coordinate bond is evident as no dissociation between the metal center (*fac*-$Re(I)(CO)_3$ moiety) and the ligand framework [DPR-X-BBN] was observed in the RP-HPLC chromatographic profiles. The aquo ligand was not observed in the ESI-MS analyses of the conjugates. These findings are consistent with co-ordinating bidentate ligands to low-valent Tc(I)/Re(I) metal centers (10, 16). All of the new Re-conjugates were obtained in very high purity and used in subsequent *in vitro* cell binding affinity studies.

Radiolabeling of the peptide conjugates was a straightforward procedure that produced the desired $[^{99m}Tc(H_2O)(CO)_3$-DPR-X-BBN$]^+$ conjugates in high radiolabeling yields. RP-HPLC-purified conjugates were used for all of the *in vitro* as well as *in vivo* studies (Figure 3). Elution of $^{99m}TcO_4^-$, followed by preparation *via* the IsoLink® radiolabeling kit to form *fac*-$[^{99m}Tc(CO)_3(H_2O)_3]^+$, afforded the $^{99m}Tc(I)$-synthon in very high yield as indicated by TLC and RP-HPLC. Reaction of *fac*-$[^{99m}Tc(CO)_3(H_2O)_3]^+$ with [DPR-X-BBN] ligands afforded the new $^{99m}Tc$-conjugates in high ~70% yield. Only trace amounts of unreacted $^{99m}TcO_4^-$ was observed in the analytical RP-HPLC ($t_R$=3.0 min) of the reaction mixture indicating little or no reoxidation of the metal center to Tc(VII). High specific activity $[^{99m}Tc(H_2O)(CO)_3$-DPR-X-BBN$]^+$ conjugates were isolated by RP-HPLC and quality control samples run with retention times of $t_R$=13.9, 13.3, 13.5, 12.4, 12.0, 12.7 and 14.2 m for X=NNN, NNN-βAla, NNN-5Ava, RRR, RRR-βAla, RRR-5Ava and SSS, respectively (Figure 4). These HPLC retention times correlate very closely to the corresponding Re(I)-conjugates demonstrating structural similarity between the metallated species. High radiochemical purity radiolabels were used for all subsequent studies as indicated by analytical RP-HPLC chromatographic profiles containing a single, high-intensity peak.

Figure 4. *RP-HPLC elution profile of* $[^{99m}Tc$-DPR-NNN-βAla-BBN$]^+$ *($t_R$=13.3 m).*

*In vitro* RP-HPLC stability studies demonstrated the stability of the coordination complex between the ligand framework and the radiometal center. The timed stability studies in BSA-containing aqueous solution at 1, 3 and 5 h time points demonstrated no noticeable dissociation of $^{99m}Tc$-radiometal from the [DPR-X-BBN] ligand framework. This was indicated by RP-HPLC chromatograms at specific time points possessing identical retention times and single, high-intensity peaks to the original chromatographic profile.

Stability studies in human serum solutions produced similar results. TLC analysis of radiolabeled conjugates after 1, 3 and 5 h incubation periods produced no activity at the solvent front, indicating little or no $^{99m}TcO_4^-$ in the solution. Radioactivity spotted near the origin of the plates showed little or no migration of conjugate in water and acetone. This indicates either in tact conjugate or serum-bound radioactivity. RP-HPLC analysis of the human serum solutions did indicate some dissociation (~25%) of the metal center from the ligand conjugate and potentially correlate with uncharacterized serum-associated $^{99m}Tc$-species. However, in tact $[^{99m}Tc(H_2O)(CO)_3$-DPR-X-

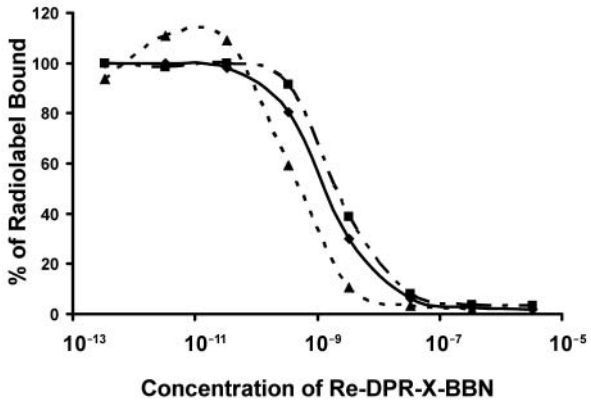


Figure 5. *$IC_{50}$ data, percentage of radiolabel bound versus concentration of [Re-DPR-X-BBN]$^+$ conjugate, for X=NNN (1.3±0.2 nM, solid line), NNN-βAla (2.2±0.1 nM, intermittently dashed line) and NNN-5Ava (3.6±2.2 nM, dashed line).*

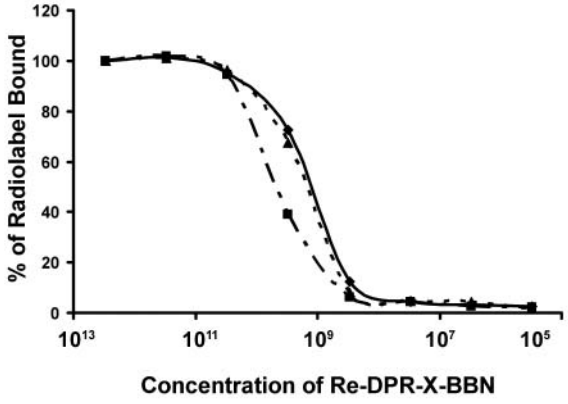


Figure 6. *$IC_{50}$ data, percentage of radiolabel bound versus concentration of [Re-DPR-X-BBN]$^+$ conjugate, for X=RRR (0.6±0.1 nM, solid line), RRR-βAla (0.2±0.02 nM, intermittently dashed line) and RRR-5Ava (0.4±0.1 nM, dashed line).*

BBN]$^+$ conjugates remained to be the major species in human serum solution. For example, for each of the new arginine or asparagines derivatives, [$^{99m}$Tc($H_2O$)($CO$)$_3$-DPR-X-BBN]$^+$ conjugate remained as the primary species in solution at concentrations of greater than 75%, as indicated by analytical RP-HPLC.

Binding affinities of the [Re($H_2O$)($CO$)$_3$-DPR-X-BBN]$^+$ conjugates for human, prostate, PC-3 cells, a cell line known to over-express the GRPr (7, 9), were demonstrated by competitive binding displacement assays *versus* $^{125}$I-Tyr$^4$-BBN radiolabeling gold standard. Nanomolar concentrations of [Re($H_2O$)($CO$)$_3$-DPR-X-Gln-Trp-Ala-Val-Gly-His-Leu-Met-$NH_2$]$^+$ were needed to reach inhibitory concentrations of 50%, $IC_{50}$, for the X=NNN, NNN-βAla, NNN-5Ava, RRR, RRR-βAla and RRR-5Ava conjugates: 1.3±0.2, 2.2±0.1, 3.6±2.2, 0.6±0.1, 0.2±0.02 and 0.4±0.1 nM respectively (Figures 5 and 6). According to this study, all of the new bombesin derivatives described herein have very high affinity for human, prostate, PC-3 cells.

The receptor-specific binding of the new [$^{99m}$Tc($H_2O$)($CO$)$_3$-DPR-X-BBN]$^+$ conjugates to surface-bound GRP receptors on PC-3 cells was determined by measuring the percentage of internalized radioactivity. Receptor binding of these GRP agonists induces endocytosis and allows for determination of receptor-specific binding and internalization of conjugate. Approximately 5-35% of the [$^{99m}$Tc($H_2O$)($CO$)$_3$-DPR-X-BBN]$^+$ activity was cell-associated. Figures 7 and 8 summarize the internalization of the [$^{99m}$Tc($H_2O$)($CO$)$_3$-DPR-X-BBN]$^+$ conjugates PC-3 cells after incubation periods of 15, 30, 45, 60, 90 and 120 m. At 120 m, all of the [$^{99m}$Tc($H_2O$)($CO$)$_3$-DPR-X-BBN]$^+$ conjugates were internalized as ~75% of the total cell-associated radioactivity. The efflux/externalization analysis took place after an initial incubation period of 45 m followed by an acid wash and secondary incubation periods of 0, 15, 30, 45, 60 and 90 m. The percentage of initial internalized activity was counted and plotted *versus* time (Figures 9 and 10). After 90 m of secondary incubation, little or no significant efflux of radioactivity out of the cell was observed.

The new series of DPR-X-BBN conjugates, where X=NNN, NNN-βAla, NNN-5Ava, RRR, RRR-βAla and RRR-5Ava, were evaluated in normal CF-1 mouse models to determine their relative biodistribution and pharmacokinetic properties *in vivo*. In these studies, a 5 μCi dose of [$^{99m}$Tc($H_2O$)($CO$)$_3$-DPR-X-BBN]$^+$ was administered to the mice intravenously. The mice were sacrificed after 1 h, as of which, the organs and tissues were excised, weighed and radioactivity measured in a well counter. The %ID/g values were then calculated (Table I). All of the conjugates demonstrated localization in normal pancreatic tissue, an organ known to express the GRPr in very high numbers in rodents (10, 16). Uptake in normal pancreas ranged from 3.65±0.51 %ID/g for [$^{99m}$Tc($H_2O$)($CO$)$_3$- DPR-RRR-BBN]$^+$ to 15.16±2.97 %ID/g for [$^{99m}$Tc($H_2O$)($CO$)$_3$-DPR-NNN-5Ava-BBN]$^+$ at 1 h *p.i.* (Table I). The extent of localization in pancreatic tissue was shown to be highest for [$^{99m}$Tc($H_2O$)($CO$)$_3$-DPR-NNN-5Ava-BBN]$^+$ and [$^{99m}$Tc($H_2O$)($CO$)$_3$-DPR-NNN-βAla-BBN]$^+$ conjugates warranting additional *in vivo* evaluation at longer time points (*vide infra*). Conjugates possessing the arginine-based linker group had significant localization in liver, ranging from 14.31±2.09 %ID/g for X=RRR to 26.20±2.68 %ID/g for X=RRR-5Ava. Asparagine-based derivatives, on the other hand, had no appreciable liver uptake. For example, only 1.25±0.16 %ID/g of conjugate accumulated in liver tissue for

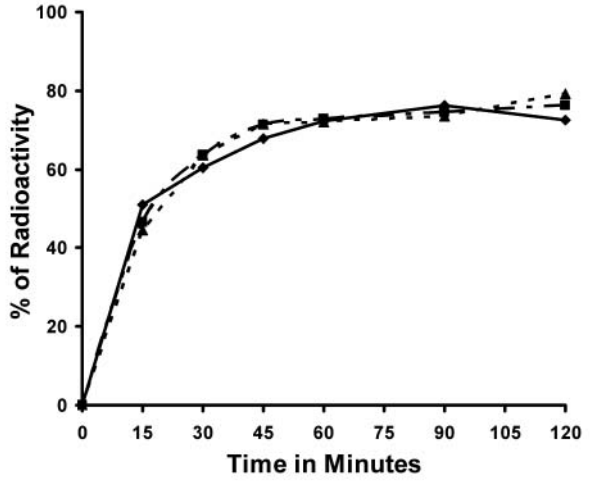


Figure 7. *Internalization data, percentage of [$^{99m}$Tc-DPR-X-BBN]$^{+}$ cell-associated radioactivity internalized versus time, for X=NNN (solid line), NNN-βAla (intermittently dashed line) and NNN-5Ava (dashed line).*

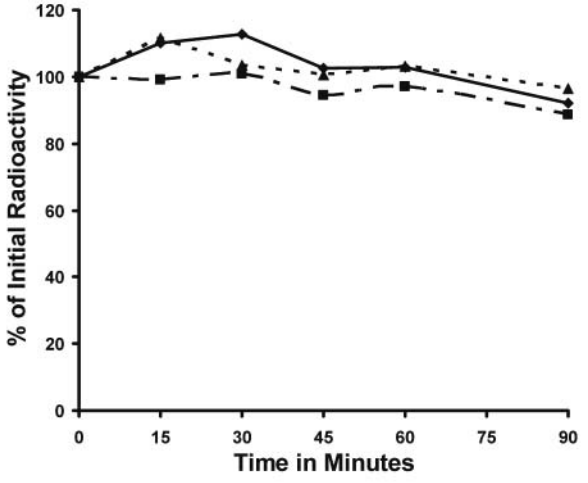


Figure 9. *Efflux data, percentage of initial [$^{99m}$Tc-DPR-X-BBN]$^{+}$ remaining internalized versus time, for X=NNN (solid line), NNN-βAla (intermittently dashed line) and NNN-5Ava (dashed line) after 15, 30, 45, 60 and 90 m secondary incubation periods.*

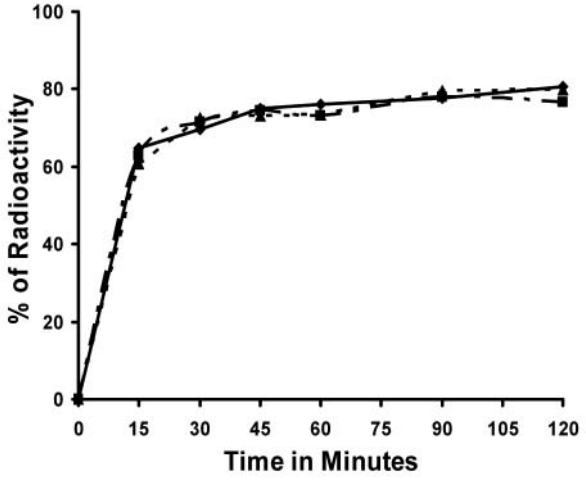


Figure 8. *Internalization data, percentage of [$^{99m}$Tc-DPR-X-BBN]$^{+}$ cell-associated radioactivity internalized versus time, for X=RRR (solid), RRR-βAla (intermittently dashed) and RRR-5Ava (dashed).*

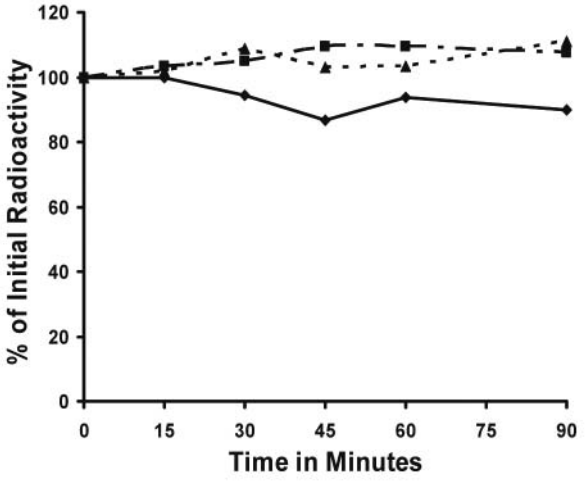


Figure 10. *Efflux data, percentage of initial [$^{99m}$Tc-DPR-X-BBN]$^{+}$ remaining internalized versus time, for X=RRR (solid line), RRR-βAla (intermittently dashed line) and RRR-5Ava (dashed line) after 15, 30, 45, 60 and 90 m secondary incubation periods.*

[$^{99m}$Tc($H_2O$)$(CO)_3$-DPR-NNN-5Ava-BBN]$^{+}$ at 1 h in *p.i.* in normal mouse models. The extent of clearance *via* the renal-urinary tract is expressed as percent injected dose. Asparagine derivatives showed a higher degree of renal-urinary clearance as compared to the arginine derivatives. For example, renal-urinary excretion was 82.2±7.50, 81.1±7.79 and 72.6±6.28 %ID for X=NNN, NNN-βAla and NNN-5Ava, respectively, while for X=RRR, RRR-βAla and RRR-5Ava %ID in urine was observed to be 50.6±4.08, 29.3±6.28 and 24.9±9.30. Kidney retention for the radiolabeled conjugates followed a similar pattern between the spacer group classes. Uptake in lung and spleen was also significantly higher for arginine *versus* that of asparagine spacer group derivatives. Very little variation of localization was observed in heart, stomach, small intestine, large intestine, muscle and blood tissues amongst the conjugates (Table I).

The superior pharmacokinetics and localization in receptor-specific tissue of [$^{99m}$Tc($H_2O$)$(CO)_3$-DPR-NNN-5Ava-BBN]$^{+}$ and [$^{99m}$Tc($H_2O$)$(CO)_3$-DPR-NNN-βAla-BBN]$^{+}$ conjugates, as compared to other conjugates reported in this study, justify additional studies in normal, CF-1 mice at 4 and 24 h *p.i.* (Figures 11 and 12). Similar

Table I. *Biodistributions in %ID/g(SD) of $^{99m}$Tc-DPR-X-BBN conjugates in CF-1, normal mice at 1 h p.i.*(16).*

| Tissue/Organ | X=NNN | X=NNN-βAla | X=NNN-5Ava | X=RRR | X=RRR-βAla | X=RRR-5Ava | X=SSS * |
|---|---|---|---|---|---|---|---|
| Heart | 0.42(0.08) | 0.33(0.11) | 0.38(0.08) | 1.27(0.09) | 1.99(0.76) | 1.94(0.24) | 0.57(0.07) |
| Lung | 0.64(0.15) | 0.65(0.19) | 0.63(0.12) | 4.00(0.44) | 5.40(1.54) | 4.81(1.05) | 0.77(0.14) |
| Liver | 1.03(0.22) | 0.78(0.15) | 0.12(0.16) | 14.3(2.1) | 16.9(5.4) | 26.2(3.67) | 2.71(0.71) |
| Kidney | 3.24(0.32) | 2.81(0.37) | 3.51(0.45) | 10.5(0.85) | 19.5(5.6) | 23.8(2.7) | 6.02(0.75) |
| Spleen | 0.43(0.17) | 0.69(0.07) | 1.12(0.56) | 3.47(0.76) | 5.17(1.29) | 6.20(0.89) | 1.48(0.38) |
| Stomach | 0.44(0.11) | 0.89(0.75) | 5.06(9.10) | 0.82(0.30) | 1.12(0.20) | 1.34(0.19) | 1.28(0.47) |
| S. Intestine | 2.83(0.42) | 3.36(0.57) | 5.61(3.11) | 2.27(0.37) | 3.64(0.82) | 3.27(0.58) | 5.81(2.61) |
| L. Intestine | 1.22(0.33) | 1.95(0.62) | 2.05(0.32) | 1.83(0.96) | 1.92(0.55) | 2.05(0.30) | 2.79(0.49) |
| Muscle | 0.19(0.08) | 0.11(0.03) | 0.18(0.00) | 0.40(0.04) | 0.90(0.30) | 0.86(0.14) | 0.28(0.14) |
| Blood | 0.79(0.12) | 0.69(0.24) | 0.78(0.13) | 1.35(0.25) | 1.62(0.41) | 1.79(0.46) | 1.41(0.22) |
| Pancreas | 6.66(0.58) | 14.1(4.1) | 15.16(3.0) | 3.65(0.51) | 10.4(3.4) | 10.3(2.2) | 16.3(1.4) |
| Urine (%ID) | 82.2(7.5) | 81.1(7.79) | 72.6(6.28) | 50.6(4.08) | 29.3(6.28) | 24.9(9.3) | 67.4(1.8) |

uptake and retention of radioactivity in tissues was observed for the two conjugates. However, some difference in localization in pancreatic tissue exists at each the 4 and 24 h time points. For example, for X=NNN-βAla receptor-mediated accumulation in pancreas was 9.43±1.69 and 3.21±0.88 %ID/g at 4 and 24 h, respectively. On the other hand, for X=NNN-5Ava uptake was significantly less with 6.00±0.70 and 1.91±0.59 %ID/g at 4 and 24 h. At 24 h, the majority of activity had cleared the body *via* the renal-urinary excretion pathway. For example, 90.58±2.36 and 91.21±2.10 %ID for X=NNN-5Ava and NNN-βAla was effectively cleared at 24 h *p.i.*.

Rapid blood clearance, excretion primarily *via* the renal/urinary pathway and high receptor-mediated pancreatic uptake of [$^{99m}$Tc($H_2O$)($CO$)$_3$-DPR-NNN-βAla-BBN]$^+$ conjugate warranted studies in tumor-bearing mouse models. To observe the extent of tumor uptake of [$^{99m}$Tc($H_2O$)($CO$)$_3$-DPR-NNN-βAla-BBN]$^+$ in living mouse models, SCID mice were xenografted with human, prostate, PC-3 cancer cells, developing viable tumors ranging from 0.09 to 0.41 grams at the time of the study. Briefly, 5 μCi doses of $^{99m}$Tc-conjugate were administered to mice. At time points of 1, 4 and 24 h *p.i.*, the mice were sacrificed, tissues were excised and counted, and the %ID/g determined. The pharmacokinetic properties of [$^{99m}$Tc($H_2O$)($CO$)$_3$-DPR-NNN-βAla-BBN]$^+$ conjugate in PC-3 tumor-bearing mice were very similar to those reported in normal mouse models (Figure 13). For example, clearance primarily *via* the renal-urinary excretion pathway was very similar to that observed in the CF-1 models. Receptor-specific pancreatic accumulation of conjugate was 19.51±3.16, 12.35±1.38, 3.95±0.72 %ID/g at 1, 4 and 24 h, respectively. Two tumors developed on each bilateral subcutaneous flank and each demonstrated specific uptake of the radiolabeled conjugate. One of the tumors showed an accumulation of 2.79±0.95, 1.44±0.37 and 0.34±0.17 %ID/g at 1, 4 and 24 h *p.i.*. The other tumor showed site-directed accumulation of 3.28±1.18, 1.76±0.53 and 0.45±0.18 %ID/g at 1, 4 and 24 h *p.i.*, respectively.

[$^{99m}$Tc($H_2O$)($CO$)$_3$-DPR-NNN-βAla-BBN]$^+$ conjugate was selected for Micro-SPECT imaging studies in PC-3 tumor-bearing mice and was compared to [$^{99m}$Tc($H_2O$)($CO$)$_3$-DPR-SSS-BBN]$^+$, a site-directed conjugate previously developed in our laboratory (Figure 14) (16). [$^{99m}$Tc($H_2O$)($CO$)$_3$-DPR-SSS-BBN]$^+$ conjugate had previously demonstrated ideal characteristics for a site-directed diagnostic radiopharmaceutical including desirable pharmacokinetics and tumor-specific accumulation (Figure 15). In addition to Micro-SPECT imaging, Micro-MRI and Micro-CT imaging were performed to anatomically correlate the *in vivo* localization of conjugate to specific tissues. For each of the new conjugates, tumors xenografted in the bilateral subcutaneous flanks of rodent models were able to be resolved. Micro-SPECT images of [$^{99m}$Tc($H_2O$)($CO$)$_3$-DPR-NNN-βAla-BBN]$^+$ conjugate (Figure 16) show significant accumulation of radioactivity in kidney and intestines, relative to tumor at 24 h *p.i.*. [$^{99m}$Tc($H_2O$)($CO$)$_3$-DPR-SSS-BBN]$^+$, on the other hand, demonstrated receptor-mediated accumulation of activity in tumor very similar to [$^{99m}$Tc($H_2O$)($CO$)$_3$-DPR-NNN-βAla-BBN]$^+$ (Figure 17). However, there was significantly less retention in the abdomen, indicating excessive washout of activity from collateral tissue at 24 h *p.i.* as compared to [$^{99m}$Tc($H_2O$)($CO$)$_3$-DPR-NNN-βAla-BBN]$^+$ conjugate.

## Discussion

The bombesin receptor super-family is comprised of four receptor subtypes: 1) The neuromedin B receptor (BB1); 2) The gastrin releasing peptide receptor (BB2); 3) The orphan receptor subtype (BB3); and 4) The bombesin receptor

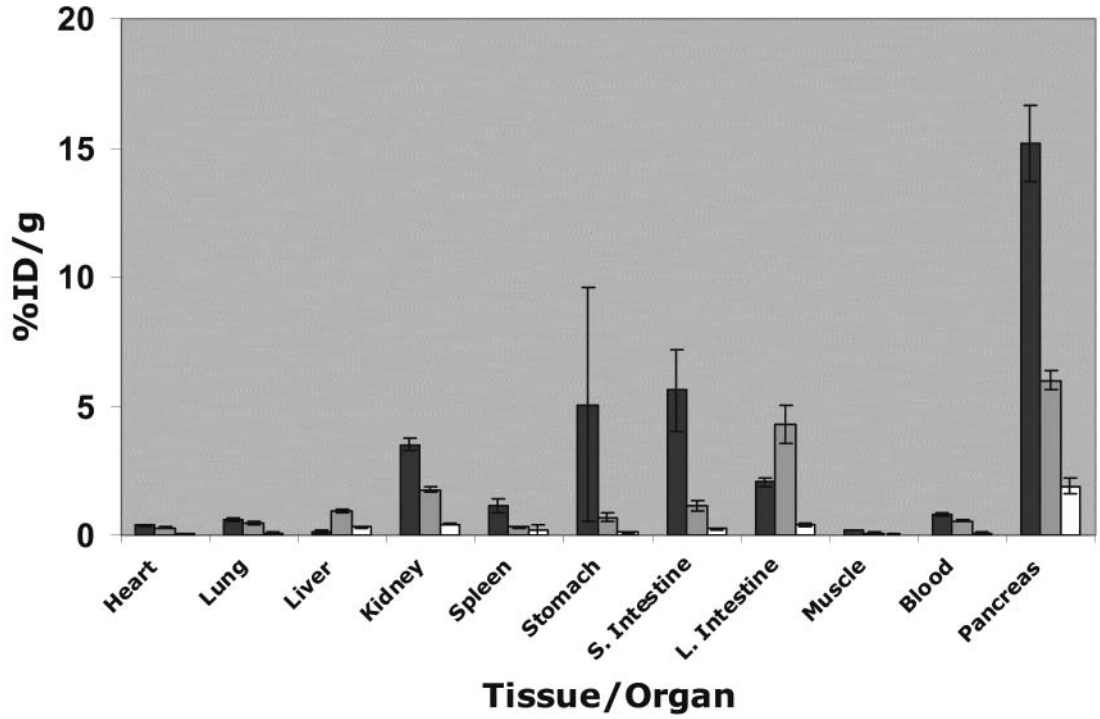


Figure 11. *In vivo biodistribution analyses, %ID/g per tissue/organ, of [$^{99m}$Tc-DPR-NNN-5Ava-BBN]$^{+}$ in CF-1 normal mice (n=5) at 1, 4 and 24 h (dark grey, light grey and white, respectively). The %ID in urine was 72.6±62.8, 84.7±3.63 and 90.6±2.36 %ID at 1, 4 and 24 h p.i., respectively.*

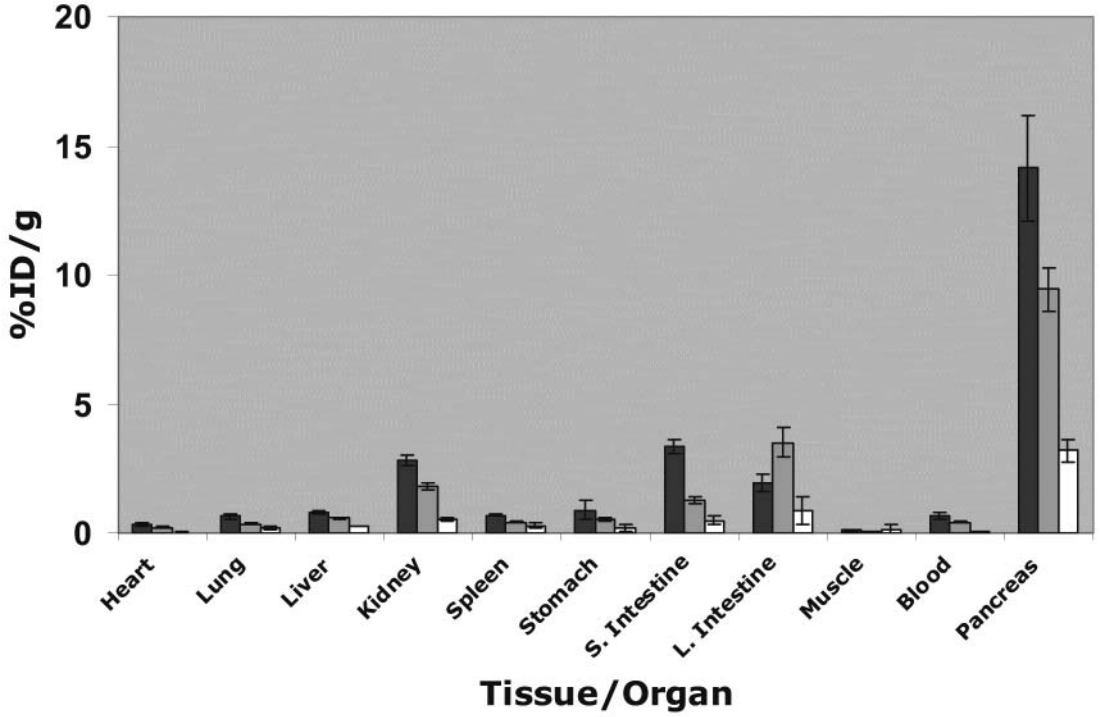


Figure 12. *In vivo biodistribution analyses, %ID/g per tissue/organ, of [$^{99m}$Tc-DPR-NNN-βAla-BBN]$^{+}$ in CF-1 normal mice (n=5) at 1, 4 and 24 h (dark grey, light grey and white, respectively). The %ID in urine was 81.1±77.9, 86.9±26.6 and 91.2±2.10 %ID at 1, 4 and 24 h p.i., respectively.*

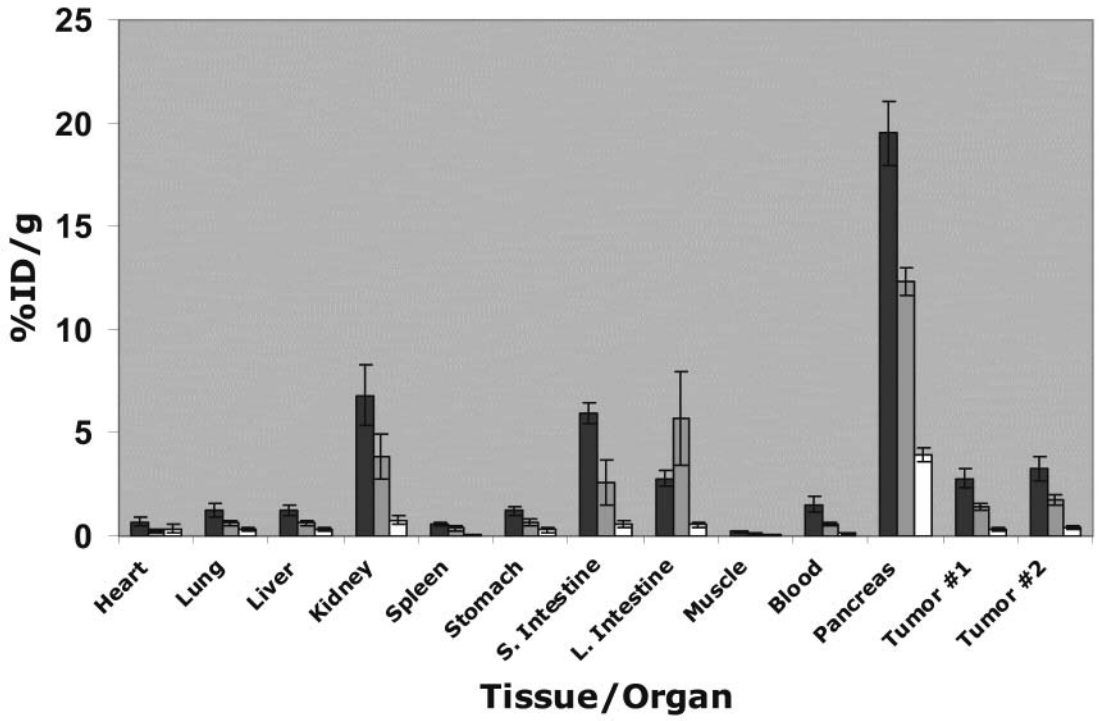


Figure 13. *In vivo biodistribution analyses, %ID/g per tissue/organ, of* $[^{99m}Tc(H_2O)(CO)_3$*-DPR-NNN-βAla-BBN]*$^+$ *in PC-3 tumor-bearing mice (n=5) at 1, 4 and 24 h (dark grey, light grey and white, respectively). The %ID in urine was 76.0±4.94, 85.9±6.40 and 92.9±0.94 %ID at 1, 4 and 24 h p.i., respectively.*

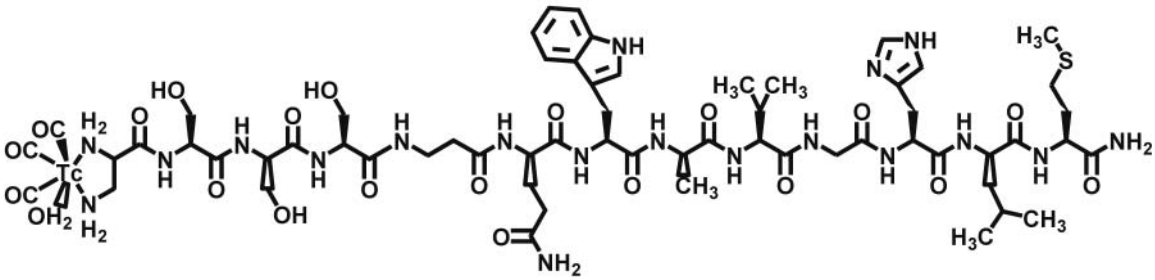

Figure 14. *Structure of* $[^{99m}Tc(CO)_3(H_2O)$*-DPR-SSS-Gln-Trp-Ala-Val-Gly-His-Leu-Met-*$NH_2]^+$.

subtype (BB4) (7, 9). Research efforts driving design and development of radiopharmaceuticals that specifically target the bombesin receptor super-family is based upon reports demonstrating over-expression of the GRP receptor subtype 2 on various human tumors or tumor cell lines that include prostate, breast, pancreatic, gastric and small cell lung cancer (7, 9). However, recent investigations also demonstrate targeting of other bombesin receptor subtypes as well. For example, Chen, Lantry, Linder *et al.*, (Bracco Research USA, Princeton, NJ) recently reported the design of $^{177}$Lu-AMBA [$^{177}$Lu- DOTA-G-(4-aminobenzoyl)-QWAVGHLM-$NH_2$], a therapy agent for treatment of prostate cancer, that specifically targets the BB1 (Neuromedin B) and BB2 (GRP) receptor subtypes of the bombesin family (38-40). Pradhan *et al.*, have developed a universal ligand (D-Tyr$^6$, β-Ala$^{11}$, Phe$^{13}$, Nle$^{14}$)bombesin(6-14) that has high affinity for BB1, BB2, BB3 and BB4 receptor subtypes (41, 42). More recently, Zhang and coworkers reported the design and development of DOTA/DTPA Pan-Bombesin derivatives that specifically target BB1, BB2 and BB3 receptor subtypes and can be radiolabeled with a host of lanthanide or lanthanide-like radioelements (43). The studies described herein are based upon previous reports of low-valent $^{99m}$Tc-conjugates designed and developed in our laboratory that specifically target the BB2 receptor subtype of the bombesin super-family (10, 16). In those reports, studies showed that conjugates of

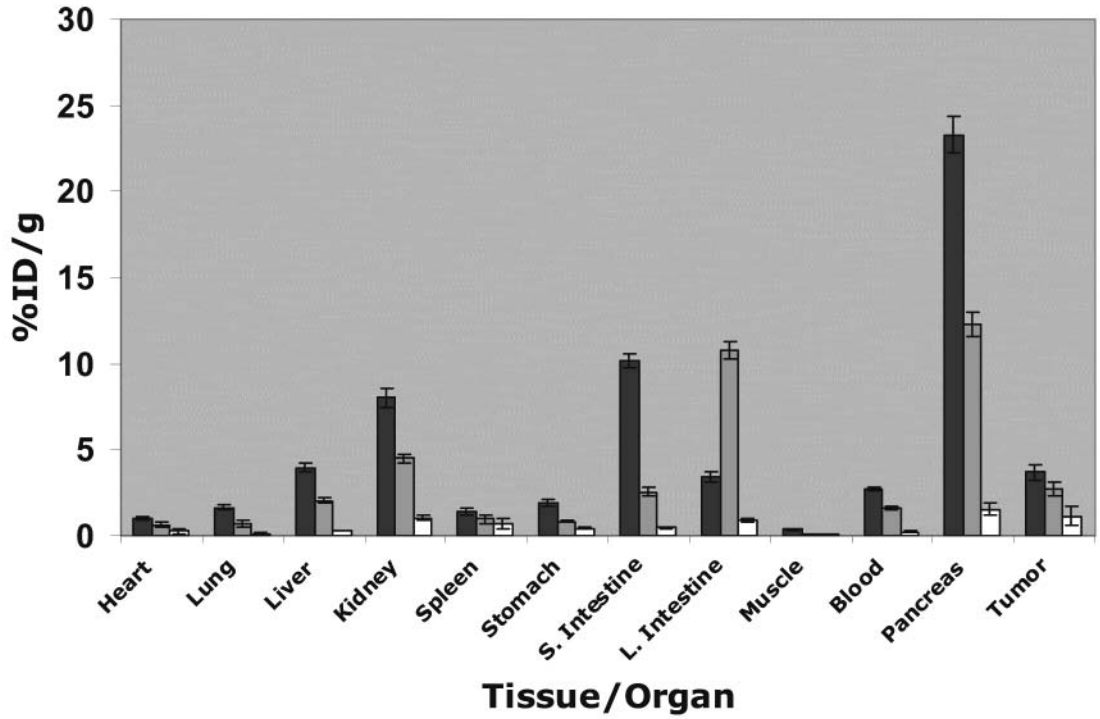


Figure 15. *In vivo biodistribution analyses, %ID/g per tissue/organ, of [$^{99m}$Tc($H_2O$)($CO_3$)-DPR-SSS-BBN]$^+$ in PC-3 tumor-bearing mice (n=5) at 1, 4 and 24 h (dark grey, light grey and white, respectively). The %ID in urine was 65.6±4.64, 75.7±2.27 and 84.5±1.75 %ID at 1, 4 and 24 h p.i., respectively (16).*

the general type [*M($H_2O$)($CO$)$_3$-DPR-X-BBN]$^+$ (where *M=$^{99m}$Tc/$^{188}$Re, DPR = a diaminoproionic acid chelating ligand framework and X = a pharmacokinetic modifier) specifically targeted BB2 receptors over-expressed on PC-3 prostate tumor xenografts. In the current study, we have made attempts to improve the *in vivo* pharmacokinetics of these conjugates by focusing solely upon the spacer/pharmacokinetic modifier groups X to chemically tune the hydrophilicity/hydrophobicity of the radiopharmaceutical.

[DPR-X-BBN] conjugates, where X=NNN, NNN-βAla, NNN-5Ava, RRR, RRR-βAla, RRR-5Ava, or SSS, were synthesized by SPPS, purified by RP-HPLC and fully characterized by ESI-MS. All of the new conjugates co-ordinate technetium and rhenium metal centers in bidentate fashion through the primary amine nitrogen donor atoms of diaminopropionic acid, giving the metal complexes sufficient stability for *in vivo* radiochemical investigations. In this study, we were to effectively show that the new [DPR-X-BBN] conjugates could be radiolabeled in very high yield upon simple heating with the *fac*-$^{99m}$Tc($CO$)$_3$($H_2O$)$_3$-synthon. Metallation of the new conjugates with nonradioactive rhenium and characterization by ESI-MS provided strong chemical-structural evidence as to the chemical constitution of the new conjugates. Peak matching RP-HPLC chromatographic profiles of non-radioactive Re-conjugates with corresponding $^{99m}$Tc-conjugates demonstrated the similarity in structure between the two species. All of the new conjugates were stable in human serum for an extended period, demonstrating the ability of the nitrogen-based diaminopropionic acid chelator to effectively stabilize the metal center against transmetallation reactions to serum-based proteins. For example, [$^{99m}$Tc($H_2O$)($CO$)$_3$-DPR-X-BBN]$^+$ conjugates were stable (≥75% of conjugate intact) for periods up to 5 h post incubation in human serum as indicated by RP-HPLC. RP-HPLC time point evaluation of all of the new conjugates demonstrated effective stability for periods as long as 5 h as well, with little or no dissociation of the metal center from ligand conjugate. $IC_{50s}$ for all of the [Re($H_2O$)($CO$)$_3$-DPR-X-BBN]$^+$ conjugates were in the single-digit nanomolar range, demonstrating very high affinity of these conjugates for the GRPr *in vitro*.

Maximizing uptake and residualization of radioactivity in human tumor tissue is essential in order to optimize the diagnostic/therapeutic efficacy of radiolabeled targeting vectors of this general type. Results of internalization studies in GRP receptor-expressing PC-3 cells showed that most of the radioactivity was not surface bound and was not lost from the cells upon incubation in pH 2.5 buffer. These studies further indicate high selectivity and affinity of

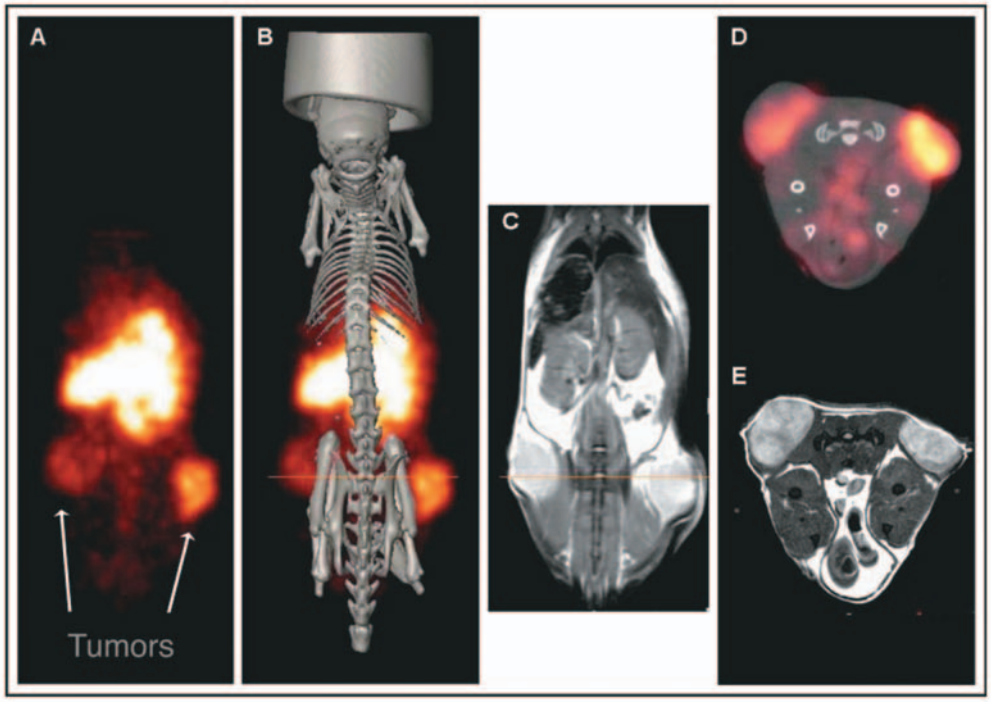


Figure 16. *In vivo SPECT/CT and MRI imaging studies of the [$^{99m}$Tc-DPR-NNN-βAla-BBN]$^{+}$ conjugate in a PC-3 tumor-bearing mouse. (A) Micro-SPECT imaging shows tumor uptake of [$^{99m}$Tc-DPR-NNN-βAla-BBN]$^{+}$. (B) Superimposed micro-SPECT map and micro-CT skeleton image. (C) Coronal image of micro-MRI shows high resolution and excellent soft tissue contrast of the mouse anatomy. Relative higher uptake was observed in kidneys and intestines compared to the tumors. No uptake was observed in liver, lung and brain. (D) A cross section of micro-SPECT/CT images showing functional imaging of tumor uptake. (E) The corresponding high-resolution micro-MRI image correlates the tumor anatomical features to (D).*

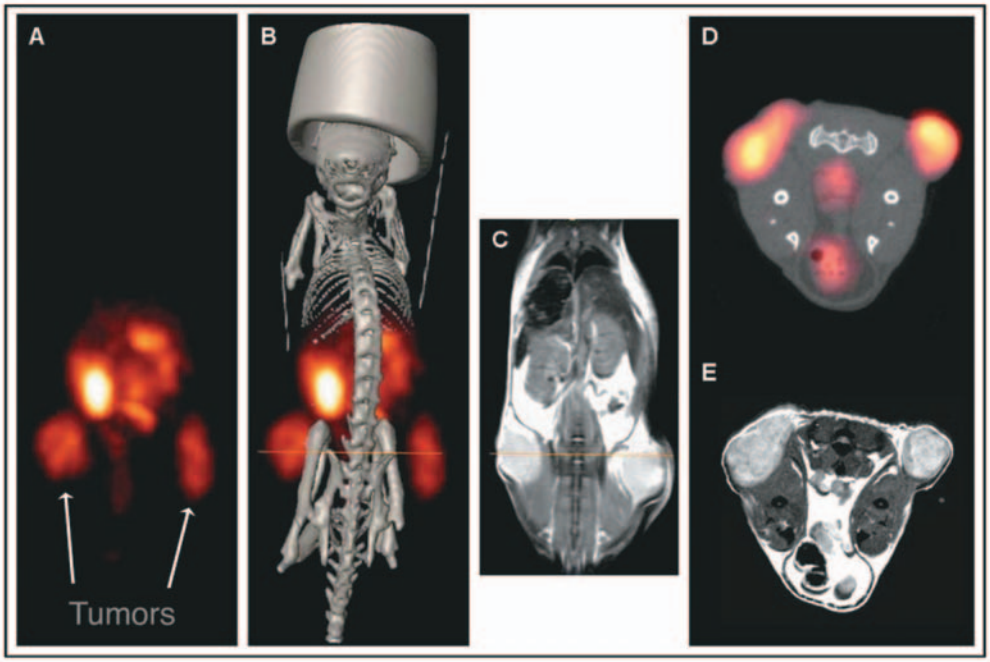


Figure 17. *In vivo SPECT/CT and MRI imaging studies of the [$^{99m}$Tc-DPR-SSS-BBN]$^{+}$ conjugate in a PC-3 tumor-bearing mouse. (A) Micro-SPECT imaging shows tumor uptake of [$^{99m}$Tc-DPR-SSS-BBN]$^{+}$. (B) Superimposed micro-SPECT map and micro-CT skeleton image. (C) Coronal image of micro-MRI. Good tumor uptake was obtained, some uptake was observed in kidneys, no uptake was observed in liver, lung and brain. (D) A cross section of micro-SPECT/CT images showing functional imaging of tumor uptake. (E) The corresponding high-resolution micro-MRI image correlates the tumor anatomical features to (D).*

$[^{99m}Tc(H_2O)(CO)_3$-DPR-X-BBN$]^+$ conjugates for GRP receptor-expressing cells. The mechanism of localization and residualization of agonist conjugates of this type is presumably receptor-mediated endocytosis. Externalization assays demonstrated little or no significant efflux of radioactivity out of the cell at specific time points, demonstrating the agonistic behavior of these conjugates.

*In vivo* evaluation of $[^{99m}Tc(H_2O)(CO)_3$-DPR-X-BBN$]^+$ conjugates demonstrated rapid clearance from the bloodstream. Excretion of conjugate was greatly influenced by the amino acid pharmacokinetic modifier that was chosen. For example, for X=NNN, excretion of conjugates were primarily *via* the renal-urinary pathway. On the other hand, for X=RRR, excretion was primarily *via* the hepatobiliary pathway. This is easily explained by the polar-uncharged nature of asparagines as compared to the higher molecular weight and basic amino acid arginine. The additional aliphatic βAla and 5-Ava linkers for some of the conjugates did have some effect on the pharmacokinetics. For example, for X=RRR, the presence of either βAla or 5-Ava reduced renal-urinary excretion by as much as 50%. Normal pancreatic uptake in rodents is used as a quality control mechanism to test for effective targeting of the GRPr in normal rodent models. The pancreas has been shown to express the GRPr in very high numbers in rodent models (10, 16). However, there is very little expression of GRPr on normal pancreas in humans. Reubi has reported expression of functional BB3 receptors in islets of normal human pancreas (44). However, minimal expression of BB1 and BB2 receptors has been identified in normal human pancreatic tissue (44). On the other hand, GRP receptor mRNA is expressed in normal human pancreatic cells (45), although the expression of mRNA for the GRPr may not be synonymous with the presence of functional GRPr (46). All of the new conjugates demonstrated some localization and accumulation in normal pancreatic tissue at 1 h *p.i.,* demonstrating the effectiveness of these conjugates to target the GRPr *in vivo*.

Additional studies in normal, CF-1 mice at 4 and 24 h *p.i.* for $[^{99m}Tc(H_2O)(CO)_3$-DPR-NNN-βAla-BBN$]^+$ conjugate indicated high pancreas uptake with clearance properties suited for further studies in tumor-bearing rodent models. High tumor uptake and retention of $[^{99m}Tc(H_2O)(CO)_3$-DPR-NNN-βAla-BBN$]^+$ in GRP receptor-expressing PC-3, prostate tumors was observed. For example, accumulation of radioactivity in tumor tissue was 2.50±0.29 and 1.62±0.44 %ID/g at 1 and 4 h *p.i.*, respectively. The high tumor and pancreatic uptake in rodent models was a reflection of the high binding affinity of this conjugate for the GRPr. For example, receptor-specific pancreatic accumulation of conjugate was 19.51±3.16, 12.35±1.38, 3.95±0.72 %ID/g at 1, 4 and 24 h *p.i.*, respectively. Tumor uptake and retention was of 3.01±1.51, 1.60±0.65 and 0.40±0.17 %ID/g at 1, 4 and 24 h *p.i.,* and were less than $[^{99m}Tc(H_2O)(CO)_3$-DPR-SSS-BBN$]^+$ conjugate, a site-directed molecule previously synthesized in our laboratory (16). For example, uptake and retention of tumor activity was 3.68±0.92, 2.71±0.78 and 1.14±1.07 %ID/g for $[^{99m}Tc(H_2O)(CO)_3$-DPR-SSS-BBN$]^+$ conjugate at 1, 4 and 24 h *p.i.,* respectively (16). From these studies, it is clearly evident that the highly polarizable NNN-βAla pharmacokinetic modifier of $[^{99m}Tc(H_2O)(CO)_3$-DPR-NNN-βAla-BBN$]^+$ conjugate influenced rapid clearance from whole blood and immediate excretion *via* the renal-urinary pathway (%ID in urine = 81.1±7.79 at 1 h *p.i.*). Therefore, multi-pass extraction of conjugate does not occur, lessening uptake and accumulation of activity in tumor in rodent models as compared to $[^{99m}Tc(H_2O)(CO)_3$-DPR-SSS-BBN$]^+$ (%ID in urine = 67.4±1.80 at 1 h *p.i.*).

Tumor accumulation for each of the conjugates where X = SSS or NNN-βAla is maintained even at 24 h post injection demonstrating receptor-mediated transport and subsequent intracellular trapping of this conjugate in GRP receptor-expressing cells. Micro-SPECT images of $[^{99m}Tc(H_2O)(CO)_3$-DPR-NNN-βAla-BBN$]^+$ conjugate (Figure 16) show significant accumulation of radioactivity in kidney and intestines relative to tumor at 24 h *p.i.* $[^{99m}Tc(H_2O)(CO)_3$-DPR-SSS-BBN$]^+$ (Figure 17), demonstrated receptor-mediated accumulation of activity in tumor very similar to $[^{99m}Tc(H_2O)(CO)_3$-DPR-NNN-βAla-BBN$]^+$. However, higher accumulation and retention of conjugate in tumor at 24 h *p.i.* and washout of activity from collateral tissue in the abdomen (kidneys and intestine) allowed for higher contrast, resolvable images at 24 h *p.i.* as compared to $[^{99m}Tc(H_2O)(CO)_3$-DPR-NNN-βAla-BBN$]^+$ conjugate. This retention in normal tissue is presumably influenced by the non-metabolizable βAla linking moiety present in $[^{99m}Tc(H_2O)(CO)_3$-DPR-NNN-βAla-BBN$]^+$ conjugate. These studies show $[^{99m}Tc(H_2O)(CO)_3$-DPR-SSS-BBN$]^+$ conjugate to be superior to $[^{99m}Tc(H_2O)(CO)_3$-DPR-NNN-βAla-BBN$]^+$ for imaging prostate tumors of the lower abdomen. In conclusion, these studies have demonstrated the potential utility of either $[^{99m}Tc(H_2O)(CO)_3$-DPR-NNN-βAla-BBN$]^+$ or $[^{99m}Tc(H_2O)(CO)_3$-DPR-SSS-BBN$]^+$ to effectively image prostate tumors *in vivo*. Choice of pharmacokinetic modifier has a direct influence on the *in vivo* pharmacokinetics and biodistribution of radioactivity in site-directed conjugates of this type. The $[^{99m}Tc(H_2O)(CO)_3$-DPR-X-BBN$]^+$ conjugates described in this study were of very high specific activity and were kinetically inert under stringent *in vivo* conditions. Furthermore, these conjugates showed extraordinary stability *in vitro* and *in vivo*, retaining biological activity with very high selectivity and affinity for the GRP receptor. Development strategies are currently underway in order to formulate kit preparation for conjugates of this type for clinical application in the diagnosis of human prostate cancer.

## Acknowledgements

This material is the result of work supported with resources and the use of facilities at the Harry S. Truman Memorial Veterans' Hospital. Columbia, MO, 65201 and the University of Missouri-Columbia School of Medicine, Columbia, MO 65211, USA. This work was funded in part by grants from The United States Department of Veterans' Affairs VA Merit Award and the National Institute of Biomedical Imaging and Bioengineering (1R21EB000833-01).

## References

1 Rogers BE, Bigott HM, MCCarthy DW, Della Manna D, Kim J, Sharp T and Welch MJ: MicroPET imaging of a gastrin-releasing peptide receptor-positive tumor in a mouse model of human prostate cancer using a $^{64}$Cu-labeled bombesin analogue. Bioconjug Chem *14*: 756-763, 2003.

2 Boerman OC, Oyen WJG and Corstens FHM: Radio-labeled receptor-binding peptides: a new class of radiopharmaceuticals. Sem Nucl Med *30*: 195-208, 2000.

3 Giblin MF, Wang N, Hoffman TJ, Jurisson SS and Quinn TP: Design and characterization of alpha-melanotropin peptide analogs cyclized through rhenium and technetium metal coordination. Proc Natl Acad Sci USA *95*: 12814-12818, 1998.

4 Lewis JS, Lewis MR, Srinivasan A, Schmidt MA, Wang J and Anderson CJ: Comparison of Four $^{64}$Cu-labeled somatostatin analogues *in vitro* and in a tumor bearing rat model: evaluation of new derivatives for positron emission tomography imaging and targeted radiotherapy. J Med Chem *42*: 1341-1347, 1999.

5 Liu S and Edwards DS: $^{99m}$Tc-Labeled small peptides as diagnostic radiopharmaceuticals. Chem Rev *99*: 2235-2268, 1999.

6 Cutler CS, Smith CJ, Ehrhardt GJ, Tyler TT, Jurisson SS and Deutsch E: Current and potential therapeutic uses of Lanthanide radioisotopes. Cancer Biother Radiopharm *15(6)*: 531-545, 2000.

7 Smith CJ, Volkert WA and Hoffman TJ: Radiolabeled peptide conjugates for targeting of the bombesin receptor superfamily subtypes. Nucl Med Biol *32(7)*: 733-740, 2005.

8 Giblin MF, Veerendra B and Smith CJ: Radiometallation of receptor-specific peptides for diagnosis and treatment of human cancer *in vivo*. New Anticancer Agents: *In Vitro* and *In Vivo* Evaluation *19*: 9-30, 2005.

9 Smith CJ, Volkert WA and Hoffman TJ: Gastrin releasing peptide (GRP) receptor targeted radiopharmaceuticals: a concise update. Nucl Med Biol *30*: 861-868, 2003.

10 Smith CJ, Sieckman GL, Owen NK, Hayes DL, Mazuru DG, Volkert WA and Hoffman TJ: Radiochemical investigations of [$^{188}$Re($H_2O(CO)_3$-diaminopropionic aid-SSS-bombesin(7-14)$NH_2$]: syntheses, radiolabeling and *in vitro*/*in vivo* GRP receptor targeting studies. Anticancer Res *23*: 63-70, 2003.

11 Eary JF, Schroff RW, Abrams PG, Fritzberg AR, Morgan AC, Kasina S, Reno JM, Srinivasan A, Woodhouse CS and Wilbur DS: Successful imaging of malignant melanoma with technetium-99m-labeled monoclonal antibodies. J Nucl Med *30*: 25-32, 1989.

12 Fritzberg AR and Wilbur DS: Radiolabeling of antibodies for targeted diagnostics. *In*: Targeted Delivery of Imaging Agents. Boca Raton, FL, CRC Press, Inc., pp. 83-101, 1995.

13 Goldenberg DM and Larson SM: Radioimmunodetection in cancer identification. J Nucl Med *33*: 803-814, 1992.

14 Press OW, Appelbaum FR, Early JF and Bernstein ID: Radiolabeled antibody therapy of lymphomas. Biolog Ther of Cancer Update *4*: 1-13, 1994.

15 Jain RK: Delivery of novel therapeutic agents in tumors: physiological barriers and strategies. J Natl Cancer Inst *81*: 570-576, 1989.

16 Smith CJ, Sieckman GL, Owen NK, Hayes DL, Mazuru DG, Kannan R, Volkert WA and Hoffman TJ: Radiochemical investigations of GRP receptor-specific [$^{99m}$Tc(X)$(CO)_3$-Dpr-Ser-Ser-Ser-Gln-Trp-Ala-Val-Gly-His-Leu-Met-($NH_2$)]: in PC3, tumor-bearing, rodent models: syntheses, radiolabeling, and *in vitro*/*in vivo* studies where Dpr = 2,3-diaminopropionic acid and X= $H_2O$ or $P(CH_2OH)_3$. Cancer Res *63*: 4082-4088, 2003.

17 Smith CJ, Gali H, Sieckman GL, Higginbothman C, Volkert WA and Hoffman TJ: Radiochemical investigations of $^{99m}$Tc-$N_3S$-X-BBN[7-14]$NH_2$: an *in vitro*/*in vivo* structure-activity relationship study where X = 0, 3, 5, 8, and 11-carbon tethering moteties. Bioconj Chem *14*: 93-102, 2003.

18 Faintuch BL, Santos RLSR, Souza ALFM, Hoffman TJ, Greeley M and Smith CJ: $^{99m}$Tc-HYNIC-Bombesin(7-14)$NH_2$: radiochemical evaluation with co-ligands EDDA(EDDA = ethylenediamine-N, N'-diacetic acid), tricine, and nicotinic acid. Synthesis and Reactivity in Inorganic, Metal-Organic and Nano-Metal Chemistry *35*: 43-51, 2005.

19 Smith CJ, Gali H, Sieckman GL, Hayes DL, Owen NK, Mazuru DG, Volkert WA and Hoffman TJ: Radiochemical investigations of $^{177}$Lu-DOTA-8-AOC-BBN(7-14)$NH_2$: an *in vitro*/*in vivo* assessment of the targeting ability of this new radiopharmaceutical for PC-3 human prostate cancer cells. Nuclear Medicine & Biology *30(2)*: 101-109, 2003.

20 Decristoforo C and Mather SJ: The influence of chelator on the pharmacokinetics of $^{99m}$Tc-labeled peptides. Q J Nucl Med *46*: 195-205, 2002.

21 Alves A, Correia JDG, Santos I, Veerendra B, Sieckman GL, Hoffman TJ, Rold TL, Figureroa SD, Retzloff L, McCrate J, Prasanphanich A and Smith CJ: Pyrazolyl conjugates of bombesin: a new tridentate ligand framework for the stabilization of the *fac*-[$M(CO)_3$]+ moiety. Nuclear Medicine & Biology *33*: 625-634, 2006.

22 Lewis JS, Lewis MR, Srinivasan A, Schmidt MA, Wang J, and Anderson CJ: Comparison of four $^{64}$Cu-labeled somatostatin analogues *in vitro* and in a tumorbearing rat model: evaluation of new derivatives for positron emission tomography imaging and targeted radiotherapy. J Med Chem *42*: 1341-1347, 1999.

23 Stolz B, Smith-Jones PM, Weckbecker G, Albert R, Knecht H, Haller R, Tolcsvai L, Hofman G, Pollehn K and Bruns C: Radiotherapy with yttrium-90 labeled DOTATyr3- octreotide in tumor bearing rodents. J Nucl Med *38*: 18p, 1997.

24 Anderson CJ and Welch MJ: Radiometal-labeled agents (non-technetium) for diagnostic imaging. Chem Rev *99*: 2219-2234, 1999.

25 Okarvi SV: Recent developments in $^{99m}$Tc-labelled peptide-based radiopharmaceuticals: an overview. Nuclear Medicine Communications *20*: 1093-1112, 1999.

26 Jurisson S, Berning D, Jia W and Ma D: Coordination compounds in nuclear medicine. Chem Rev *93*: 1137-1156, 1993.

27 Liu S, Edwards DS and Harris AR: A novel ternary ligand system for $^{99m}$Tc-labeling of hydrazino nicotinamide-modified biologically active molecules using imine-N-containing heterocycles and coligands. Bioconj Chem *9*: 583-595, 1998.

28 Liu S, Edwards DS and Barrett JA: $^{99m}$Tc-labeling of highly potent small peptides. Bioconj Chem *8*: 621-636, 1997.

29 Zalutsky MR and Narula AS: Radiohalogenation of a monoclonal antibody using an N-succinimidyl 3-(tri-n-butylstannyl) benzoate intermediate. Cancer Res *48*: 1446-1450, 1988.

30 Alberto R, Egli A, Schibli R, Waibel R, Abram U, Kaden TA, Schaffland A, Schwarzbach R and Schubiger PA: From $[TcO_4]^-$ to an organometallic aqua-ion: synthesis and chemistry of $[^{99m}Tc(OH_2)_3(CO)_3]^+$. *In*: Technetium, Rhenium and Other Metals in Chemistry and Nuclear Medicine. Nicolini M, and Ulderico M (eds.), SGE, Italy, 1999, pp27-34.

31 Alberto R, Schibli R, Waibel R, Abram U and Schubiger PA: Basic Aqueous Chemistry of $[M(OH_2)_3(CO)_3]^+$ (M = Re, Tc) Directed Towards Radiopharmaceutical Application. Coord Chem Rev, pp. 190-192, 901-919, 1999.

32 Nock B, Nikolopoulou A, Chiotellis E, Loudos G, Maintas D, Reubi JC *et al*: [$^{99m}$Tc] Demobesin 1, a novel potent bombesin analogue for GRP receptor-targeted tumour imaging. Eur J Nucl Med *30(2)*: 247-258, 2003.

33 Nock BA, Nikolopoulou A, Galanis A, Cordopatis P, Waser B, Reubi JC and Maina T: Potent bombesin-like peptides for GRP-receptor targeting of tumors with $^{99m}$Tc: a preclinical study. J Med Chem *48(1)*: 100-110, 2005.

34 Jurisson S and Lydon JD: Potential technetium small molecule radiopharmaceuticals. Chem Rev *99*: 2205-2218, 1999.

35 Volkert WA and Hoffman TJ: Therapeutic radiopharmaceuticals. Chem Rev *99*: 2269-2292, 1999.

36 Zalutsky MR and Bigner DD: Radioimmunotherapy with alpha-particle emitting radioimmunoconjugates. Acta Oncol *35*: 373-379, 1996.

37 Alberto R, Egli A, Abram U, Hegetschweiler K, Gramlich V and Schubiger PA: Synthesis and Reactivity of $[NEt_4]_2[ReBr_3(CO)_3]$. Formation and Structural Characterization of the Clusters $[NEt_4](Re_3(\mu_3\text{-}OH)(\mu\text{-}OH)_3(CO)_9]$ and $[NEt_4](Re_2(\mu\text{-}OH)_3(CO)_6]$ by Alkaline Titration. J Chem Soc Dalton Trans, pp. 2815-2820, 1994.

38 Lantry LE, Thomas R, Waser B, Maddalena M, Fox JS, Arunachalam T, Feng W, Eaton SM, Wedeking PW, Chen J, Linder KE, Swenson RE, Tweedle MF, Reubi JC and Nunn SD: Preclinical evaluation of $^{177}$Lu-AMBA, a DOTA conjugate that targets GRP and NMB receptor expressing tumors: Internalization, *in vivo* biodistribution, single dose radiotherapy in PC-3 tumor-bearing nude mice and *in vitro* autoradiograpy in animal and human tissues. Euro Assoc Nucl Med, Helsinki, Finland, 2004.

39 Chen J, Nguyen H, Metcalfe E, Eaton S, Arunachalam T, Raju N, Cappelletti E, Lattuada L, Cagnolini A, Maddalena M, Lantry LE, Nunn A, Swenson RE, Tweedle MF and Linder KE: Formulation and *in vitro* metabolism studies with $^{177}$Lu-AMBA; a radiotherapeutic compound that targets gastrin releasing peptide receptors. Euro Assoc Nucl Med, Helsinki, Finland, 2004.

40 Linder KE, Chen J, Feng W, Thomas R, Arunachalam T, Lantry LE, Cappelletti E, Lattuada L, Raju N, Cagnolini A, Nguyen H, Swenson RE, Nunn AD and Tweedle MF: Synthesis and *in vitro* evaluation of a $^{177}$Lu-DOTA conjugate for targeting of tumors expressing gastrin releasing peptide receptors (GRP-R). J Nuc Med *45(5)*: 169P, Abstract 482, 2004.

41 Mantey SA, Weber HC, Sainz E, Akeson M, Ryan RR, Pradhan TK, Searles RP, Spindel ER, Battey JF, Coy DH and Jensen RT: Discovery of a high affinity radioligand for the human orphan receptor, bombesin receptor subtype 3, which demonstrates that it has a unique pharmacology compared with other mammalian bombesin receptors. J Biol Chem *1272*: 26062-26071, 1997.

42 Pradhan TK, Katsuno T, Taylor JE, Kim SH, Ryan RR, Mantey SA, Donohue PJ, Weber HC, Sainz E, Battey JF, Coy DH and Jensen RT: Identification of a unique ligand which has high affinity for all four bombesin receptor subtypes. Eur J Pharm *343*: 275-287, 1998.

43 Zhang H, Chen J, Waldherr C, Hinni K, Waser B, Reubi JC and Maecke HR: Synthesis and evaluation of bombesin derivatives on the basis of pan-bombesin peptides labeled with indium-111, lutetium-177, and yttrium-90 for targeting bombesin receptor-expressing tumors. Cancer Res *64*: 6707-6715, 2004.

44 Fleischmann A, Laderach U, Friess H, Buechler MW and Reubi JC: Bombesin receptors in distinct tissue compartments of human pancreatic diseases. Laboratory Investigation *80(12)*: 1807-1817, 2000.

45 Sano H, Feighner SD, Hreniuk DL, Iwaasa H, Sailer AW, Pan J, Reitman ML, Kanatani A, Howard AD and Tan CP: Characterization of the bombesin-like peptide receptor family in primates. Genomics *84*: 139-146, 2004.

46 Van De Wiele C, Dumont F, Van Belle S, Slegers G, Peers SH and Dierckx RA: Is there a role for agonist gastrin-releasing peptide receptor radioligands in tumor imaging? Nucl Med Comm *22*: 5-15, 2001.

*Received December 12, 2006*
*Accepted December 18, 2006*